Nonparabolic multivalley balance-equation approach to high-field electron transport and impact ionization in ZnS: Comparison with full-band Monte Carlo simulations

J. C. Cao

State Key Laboratory of Functional Materials for Informatics, Shanghai Institute of Microsystem and Information Technology, Chinese Academy of Sciences, 865 Changning Road, Shanghai 200050, People's Republic of China

(Received 13 September 2003; revised manuscript received 1 December 2003; published 8 April 2004)

Extended nonparabolic multivalley balance equations including impact ionization (II) process are presented and are applied to study electron transport and impact ionization in ZnS with a Γ, X, and L conduction-band structure at high electric field up to 2000 kV/cm. Hot-electron transport properties, such as electron drift velocity, electron energy, intervalley electron transfer, and electron-hole pair generation, are calculated by taking account of the scattering from polar optical, deformation potential, and intervalley interactions. Quantitative agreement is obtained among the results for drift velocity and II coefficient derived from the present calculations, from the recent full-band Monte Carlo simulations, and from experiments, thus confirming the validity of the present multivalley nonparabolic balance-equation approach.

DOI: 10.1103/PhysRevB.69.165203 PACS number(s): 72.20.Ht, 72.20.Jv, 72.10.−d, 73.50.Fq

I. INTRODUCTION

Recently, high-field transport of ZnS has attracted a growing interest owing to its promising applications in efficient electroluminescent displays. The understanding of hot-electron transport properties of ZnS is essential for the design and operation of ZnS-based ac thin film electroluminescent devices. These devices operate in the high-field range 0.5–2.0 MV/cm and rely on the process of carrier multiplication by interband impact ionization (II). During the past decades a few attempts have been made to investigate the transport behavior of ZnS in the high-field regime. The typical technique is Monte Carlo (MC) simulation,[1–7] in which the microscopic scattering rates and the full-band structure in the entire Brillouin zone are needed. Recently, *ab initio* band-structure MC calculations for ZnS within density-functional theory have been performed by using an exact exchange formalism with local-density approximation (MC-EXX-LDA) (Ref. 7) for correlations. The exact treatment of the exchange interaction allows one to reproduce band-gap energies very accurately for a variety of semiconductor materials. As to theoretical methods for the II process in semiconductors, the analytical models widely used are the ones by Shockley,[8] Wolff,[9] and Baraff.[10] Shockley[8] assumed that ionizing carriers are those that are sufficiently ''lucky'' to drift to an energy greater than or equal to the threshold energy without experiencing any energy relaxation collisions. This idea was later developed into the lucky-electron model by Ridley[11] and improved by Wilson.[12] Wolff[9] considered that the electrons are heated entirely by an external field and by many collisions, and it is these electrons at the high-energy tail of the energy distribution which give rise to II. By combining the features of the Shockley and Wolff theories Baraff[10] later formulated a more sophisticated II model which provides a better agreement with experiment in realistic systems. To study the II process in semiconductors, Quade *et al.*[13] developed a detailed II theory including thresholds for general bands within the hydrodynamic approach. They rigorously determined the threshold energy ε_T from momentum and energy conservation for an individual electron. The electron will have a probability to produce an electron-hole pair by II process when its energy is larger than ε_T.

In this paper we present the nonparabolic multivalley balance equations including the II process[14,15] and apply them to study transport properties and II in ZnS at high electric field up to 2000 kV/cm. We have obtained the electric-field dependence of transport qualities, such as the drift velocity, electron energy, valley occupation, and II coefficient at different lattice temperatures. We compared our calculated results for electron drift velocity and II coefficient with MC simulations[5–7] and the available experiments.[16] Quantitative agreement is found, thus confirming the validity of the present multivalley nonparabolic balance-equation approach.

II. NONPARABOLIC MULTIVALLEY BALANCE EQUATIONS INCLUDING II PROCESS

Consider a semiconductor having a band structure of s valleys with an energy-wave vector relation $\varepsilon_a(\mathbf{k})$ for electrons and $\varepsilon_a^h(\mathbf{k})$ for holes in each valley ($a=1,2,\ldots,s$). According to the balance-equation theory, under the influence of a uniform electric field $\mathbf{E}$ the carrier conduction is described by the following equations for the carrier density, effective momentum, and energy balance for each valley ($a=1,2,\ldots,s$, $\hbar=1$ throughout the paper)

$$\frac{dn_a}{dt}-g_{ii}^a=\sum_{b(\neq a)}X_{ei}^{ab}+\sum_{b(\neq a)}X_{ep}^{ab}, \tag{1}$$

$$\frac{d(n_a\mathbf{v}_a)}{dt}=n_a e\mathbf{E}\cdot\mathcal{K}_a+\mathbf{A}_{ei}^a+\mathbf{A}_{ep}^a+\mathbf{A}_{ii}^a+\sum_{b(\neq a)}\mathbf{A}_{ei}^{ab}+\sum_{b(\neq a)}\mathbf{A}_{ep}^{ab}, \tag{2}$$

$$\frac{d(n_a\varepsilon_a)}{dt}=n_a e\mathbf{E}\cdot\mathbf{v}_a-W_{ep}^a-W_{ii}^a-\sum_{b(\neq a)}W_{ep}^{ab}. \tag{3}$$

The above equations are the extension of the balance equations[14,15,17] to include II process for nonparabolic semiconductors having multiple valleys. The transport state of electrons in the ath valley is described by the electron chemical potential μ_a, electron temperature T_a and lattice momentum shift $\mathbf{p}_a$. On the other hand, the drift movement and heating of hole gases are negligible in comparison with those of the electron gases so that the hole gases can be described by the lattice temperature T and a hole chemical potential μ_a^h in each valley ($a=1,2,\ldots,s$). The electron density in ath valley is given by $n_a = 1/(4\pi^3)\int d^3k f[(\varepsilon_a(\mathbf{k})-\mu_a)/T_a]$. The average velocity $\mathbf{v}_a$, the average energy ε_a, and the ensemble-averaged inverse effective mass tensor $\mathcal{K}_a$ of electron in valley a are defined respectively as $\mathbf{v}_a=\langle\nabla\varepsilon_a(\mathbf{k})\rangle$, $\varepsilon_a=\langle\varepsilon_a(\mathbf{k})\rangle$, and $\mathcal{K}_a=\langle\nabla\nabla\varepsilon_a(\mathbf{k})\rangle$, in which $\langle\cdots\rangle$ stands for the weighted integral over a Brillouin zone in $\mathbf{k}$ space: $\langle\cdots\rangle = 1/(4\pi^3 n_a)\int d^3k f\{[\bar{\varepsilon}_a(\mathbf{k})-\mu_a]/T_a\}\cdots$ with $\bar{\varepsilon}_a(\mathbf{k})\equiv\varepsilon_a(\mathbf{k}-\mathbf{p}_a)$ and $f(x)=1/[\exp(x)+1]$ the Fermi distribution function. In Eqs. (1)–(3), e is the electron charge. The frictional acceleration $\mathbf{A}_{\rm ei}^a$, $\mathbf{A}_{\rm ep}^a$ (due to impurity and phonon scatterings) and the energy-loss rate $W_{\rm ep}^a$ (due to phonon scattering), share the same expressions as those given in Ref. 17. X_{ei}^{ab} and X_{ep}^{ab} are the change rates of the carrier population in the ath valley, respectively, due to the interband electron-impurity scattering and due to the interband electron-phonon scattering. Their expressions are as follows:

$$X_{ei}^{ab}=-2n_i\sum_{\mathbf{k},\mathbf{q}}|U_{ab}(q)|^2\Pi^{ab}(\mathbf{k},\mathbf{q},0), \tag{4}$$

$$X_{ep}^{ab}=-2\sum_{\mathbf{k},\mathbf{q},\lambda}|M_{ab}(q)|^2\Lambda^{ab}(\mathbf{k},\mathbf{q},\Omega_{\mathbf{q}\lambda}), \tag{5}$$

with

$$\Pi^{ab}(\mathbf{k},\mathbf{q},\Omega)=2\pi\left[f\left(\frac{\bar{\varepsilon}_{a\mathbf{k}}-\mu_a}{T_a}\right)-f\left(\frac{\bar{\varepsilon}_{b\mathbf{k}+\mathbf{q}}-\mu_a}{T_a}\right)\right]\times\delta(\varepsilon_{a\mathbf{k}}-\varepsilon_{b\mathbf{k}+\mathbf{q}}-\Omega), \tag{6}$$

$$\Lambda^{ab}(\mathbf{k},\mathbf{q},\Omega)=\Pi^{ab}(\mathbf{k},\mathbf{q},\Omega)\left[n\left(\frac{\Omega}{T}\right)-n\left(\frac{\bar{\varepsilon}_{a\mathbf{k}}-\mu_a}{T_a}-\frac{\bar{\varepsilon}_{b\mathbf{k}+\mathbf{q}}-\mu_b}{T_b}\right)\right]+\Pi^{ab}(\mathbf{k},\mathbf{q},-\Omega)\times\left[n\left(\frac{\Omega}{T}\right)-n\left(\frac{\bar{\varepsilon}_{b\mathbf{k}+\mathbf{q}}-\mu_b}{T_b}-\frac{\bar{\varepsilon}_{a\mathbf{k}}-\mu_a}{T_a}\right)\right], \tag{7}$$

in which $\bar{\varepsilon}_{a\mathbf{k}}\equiv\bar{\varepsilon}_a(\mathbf{k})$, $n(x)=1/[\exp(x)-1]$ is the Bose distribution, n_i is the impurity density, $\Omega_{\mathbf{q}\lambda}$ stands for the energy of the λth branch phonon with wave vector $\mathbf{q}$, $U_{ab}(q)$ is the interband impurity potential, $M_{ab}(q)$ is the interband electron-phonon matrix element. In Eqs. (1)–(3), g_{ii}^a, A_{ii}^a, and W_{ii}^a are, respectively, the generation rate, II-induced acceleration, and the II-induced energy-loss rate of ath valley, which describe the contribution of the II process to electron transport. Their expressions are obtained by similar calculations for single-valley system[14]

$$\mathbf{A}_{ii}^a=4\pi\sum_{\mathbf{k},\mathbf{k}',\mathbf{q}}|M_{ii}^a(q)|^2\delta(\varepsilon_{a\mathbf{k}-\mathbf{q}}+\varepsilon_{a\mathbf{k}}^h+\varepsilon_{a\mathbf{k}'+\mathbf{q}}-\varepsilon_{a\mathbf{k}'})\times[v_a(\mathbf{k}'+q)+v_a(\mathbf{k}-\mathbf{q})-v_a(\mathbf{k}')]f\left(\frac{\bar{\varepsilon}_{a\mathbf{k}'}-\mu_a}{T_a}\right)\times\left[1-f\left(\frac{\bar{\varepsilon}_{a\mathbf{k}'+\mathbf{q}}-\mu_a}{T_a}\right)\right]\left[1-f\left(\frac{\bar{\varepsilon}_{a\mathbf{k}-\mathbf{q}}-\mu_a}{T_a}\right)\right]\times\left(1-\frac{f[(\varepsilon_{a\mathbf{k}}^h-\mu_a^h)/T]}{f[(\bar{\varepsilon}_{a\mathbf{k}'}-\bar{\varepsilon}_{a\mathbf{k}'-\mathbf{q}}-\bar{\varepsilon}_{a\mathbf{k}'+\mathbf{q}}+\mu_a)/T_a]}\right), \tag{8}$$

$$W_{ii}^a=4\pi\sum_{\mathbf{k},\mathbf{k}',\mathbf{q}}|M_{ii}^a(q)|^2\varepsilon_{a\mathbf{k}}^h\delta(\varepsilon_{a\mathbf{k}-\mathbf{q}}+\varepsilon_{a\mathbf{k}}^h+\varepsilon_{a\mathbf{k}'+\mathbf{q}}-\varepsilon_{a\mathbf{k}'})\times f\left(\frac{\bar{\varepsilon}_{a\mathbf{k}'}-\mu_a}{T_a}\right)\left[1-f\left(\frac{\bar{\varepsilon}_{a\mathbf{k}'+\mathbf{q}}-\mu_a}{T_a}\right)\right]\times\left[1-f\left(\frac{\bar{\varepsilon}_{a\mathbf{k}-\mathbf{q}}-\mu_a}{T_a}\right)\right]\times\left(1-\frac{f[(\varepsilon_{a\mathbf{k}}^h-\mu_a^h)/T]}{f[(\bar{\varepsilon}_{a\mathbf{k}'}-\bar{\varepsilon}_{a\mathbf{k}'-\mathbf{q}}-\bar{\varepsilon}_{a\mathbf{k}'+\mathbf{q}}+\mu_a)/T_a]}\right), \tag{9}$$

$$g_{ii}^a=4\pi\sum_{\mathbf{k},\mathbf{k}',\mathbf{q}}|M_{ii}^a(q)|^2\delta(\varepsilon_{a\mathbf{k}-\mathbf{q}}+\varepsilon_{a\mathbf{k}}^h+\varepsilon_{a\mathbf{k}'+\mathbf{q}}-\varepsilon_{a\mathbf{k}'})\times f\left(\frac{\bar{\varepsilon}_{a\mathbf{k}'}-\mu_a}{T_a}\right)\left[1-f\left(\frac{\bar{\varepsilon}_{a\mathbf{k}'+\mathbf{q}}-\mu_a}{T_a}\right)\right]\times\left[1-f\left(\frac{\bar{\varepsilon}_{a\mathbf{k}-\mathbf{q}}-\mu_a}{T_a}\right)\right]\times\left(1-\frac{f[(\varepsilon_{a\mathbf{k}}^h-\mu_a^h)/T]}{f[(\bar{\varepsilon}_{a\mathbf{k}'}-\bar{\varepsilon}_{a\mathbf{k}'-\mathbf{q}}-\bar{\varepsilon}_{a\mathbf{k}'+\mathbf{q}}+\mu_a)/T_a]}\right), \tag{10}$$

in which the Fourier representations of the band-band Coulomb interaction matrix element $M_{ii}^a(q)$ in the ath valley is given by

$$M_{ii}^a(q)=\frac{e^2}{\epsilon_0(q^2+q_0^2)}\frac{I_{cc}I_{cv}}{\kappa}, \tag{11}$$

with a dielectric constant κ, and a reciprocal screening length $q_0=\sqrt{n_a e^2/\kappa\epsilon_0 T_a}$. I_{cc} and I_{cv} are overlap integrals of conduction-conduction and conduction-valence bands, respectively. The overall electron average velocity and the average energy are obtained by $v_d=\Sigma_a n_a v_a/n$ and $\varepsilon=\Sigma_a n_a\varepsilon_a/n$, respectively, with $n=\Sigma_a n_a$ the total electron density of the system. The electron-hole generation rate in the whole electron system is expressed by

$$g_{ii}=\frac{\sum_a n_a g_{ii}^a}{n}, \tag{12}$$

and the II coefficient of the whole electron system is given by

$$\alpha_{ii}=\frac{g_{ii}}{nv}. \tag{13}$$

III. HIGH-FIELD TRANSPORT AND IMPACT IONIZATION IN ZNS

We have performed a quasi-steady-state calculation of carrier transport in bulk ZnS by assuming that the left-hand sides of Eqs. (1)–(3) (in which $s=3$) equal zero in the field range 0–2000 kV/cm. In the calculations, we evaluated the expressions in Eqs. (4)–(10) by the Gauss integral method, and use the Newton iteration method to solve the equations. In this quasi-steady-state case, since the momentum- and energy-relaxation times are much shorter than the carrier-number relaxation time, the average electron velocity and electron energy become steady while the total number of carriers is still increasing due to II process with a constant rate, namely, the electron-hole pair generation rate g_{ii}^a $(=dn_a/dt)$. We use a three-valley model: Γ, X, and L valleys, for ZnS conduction band. We solved eight equations for the Γ, L, and X valleys, i.e., $a=1$, 2, and 3. The eight basic quantities that we solved are: electron velocities (v_1, v_2, and v_3), electron temperatures (T_1, T_2, and T_3), and valley population percentages (N_1 and N_2, then obtaining $N_3=1-N_1-N_2$). The Kane-type nonparabolic energy-wave vector relation is used for all three conduction bands. The scattering mechanisms considered here are electron-phonon scattering from the polar optical, deformation potential, and intervalley interactions. Impact ionization is regarded as an additional scattering mechanism. The material parameters used in the calculations for ZnS are listed in Table I, which are from Refs. 5 and 7.

In Fig. 1 we show the calculated electron drift velocities v_d (open circles) as a function of electric field E in ZnS at lattice temperature $T=300$ K. Results from MC simulation by using the empirical pseudopotential method (MC-EPM, solid circles),[6] recent MC simulation MC-EXX-LDA (solid triangles),[7] and experimental data[16] are also shown for comparison. It can be found that our calculated results are in a good agreement with the recent MC simulations MC-EXX-LDA by considering the details of the realistic band structure of ZnS. In Fig. 2 we show the corresponding valley occupations as a function of the electric field in ZnS at $T=300$ K. It can been seen that for an electric field below the threshold value $E_{\rm cri}\simeq 170$ kV/cm for the negative differential velocity (NDV), more than 99% electrons are distributed in the Γ valley, and for an electric field above this threshold the population of the Γ valley decreases gradually, while those of the X and L valleys increase. At $E=1000$ kV/cm, the populations in the X and L valleys are 38% and 4.2%, respectively.

To see the temperature dependence of transport properties, we show in Fig. 3 the calculated average electron velocity v_d of the whole system (left axis) and the normalized electron temperature, T_1/T, for the Γ valley (right axis) as a function of the electric field E in ZnS at different lattice temperatures $T=77$, 180, and 300 K, respectively. It is indicated from Fig. 3 that the electron drift velocity at low temperature is greater than that at high temperature. The reason is that the scatterings from electron-phonon interactions become weak at low temperature. In Fig. 4 we show the average electron energies as a function of the electric field in ZnS at different lattice temperatures $T=77$, 180, and 300 K, re-

TABLE I. ZnS parameters used in the calculations.

Band gap (eV)	3.68		
Material density (g/cm^3)	4.08		
Effective hole effective mass (m_0)	1.0		
Longitudinal sound velocity (10^5 cm/s)	5.2		
Static dielectric constant	8.31		
High frequent dielectric constant	5.13		
Acoustic deformation potential (eV)	4.9		
Optical phonon energy (meV)	43.0		
Valley	Γ	X	L
Electron effective mass (m_0)	0.34	0.4	0.222
Nonparabolicity (eV^{-1})	0.69	0.65	0.36
Valley separation (eV) (relative to Γ valley)	0	0.69	0.95
Number of equivalent valleys	1	4	3
Intervalley deformation potential (10^9 eV/cm)			
From Γ	0.0	1.0	1.0
From X	1.0	0.9	0.9
From L	1.0	1.0	0.9
Intervalley phonon energy (meV)			
From Γ	0.0	26.7	27.9
From X	27.9	27.3	27.9
From L	26.7	26.7	27.3

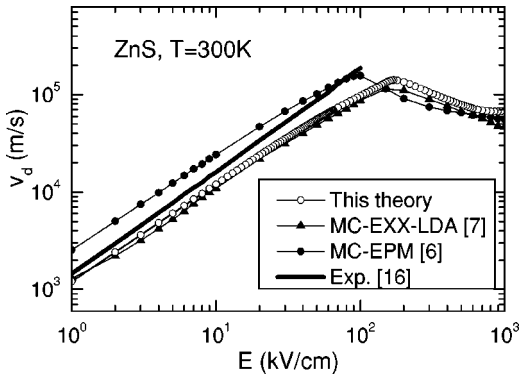

FIG. 1. Calculated electron drift velocities (open circles) v_d as a function of electric field E in ZnS at lattice temperatures $T=300$ K. Results from MC simulation by using the empirical pseudopotential method (MC-EPM, solid circles) (Ref. 6), recent MC simulation by using an exact exchange formalism with local-density approximation (MC-EXX-LDA, solid triangles) (Ref. 7) for correlations, and experimental data (thick line) (Ref. 16) are also shown for comparison.

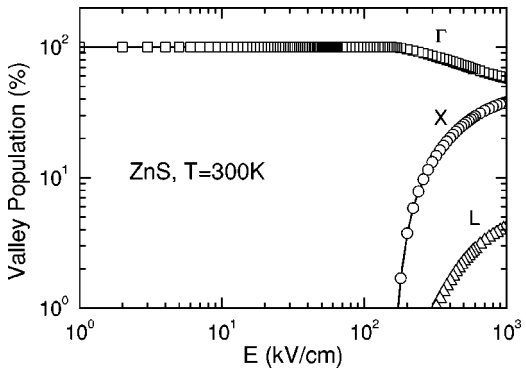

FIG. 2. Valley occupations are shown as a function of the electric field E in ZnS at $T=300$ K. At the electric field $E=1000$ kV/cm, the populations in the X and L valleys are 38% and 4.2%, respectively.

spectively. In connection with the velocity-field curve, the relation of electron energy vs electric field provides some more physical insight into transport properties, especially into the II process. The dependence of the average total energy on electric field in ZnS shows a behavior typical for compound semiconductor materials in that the average energy increases abruptly by almost an order of magnitude near the threshold field E_{cri} for NDV with a flattened shape at either the low- or the high-field ranges.

In Fig. 5 we show the calculated II coefficient α_{ii} of ZnS as a function of the inverse electric field at $T=300$ K. The solid squares is the ensemble Monte Carlo (EMC) simulation results for ZnS from Ref. 5, and the dashed line shows the results for ZnS from device modeling assuming that all carrier multiplication is due to the II process.[5] In addition, to further check the present II approach, we have also calculated and shown in Fig. 5 the II coefficients of GaAs at $T=300$ K. The experimental results by Bulman *et al.*[18] are also plotted for comparison. Good quantitative agreements are found between the present calculated results and the ones from MC simulations and the available experiments both for ZnS and for GaAs, thus confirming the validity of the present II model. In order to discuss the dependence of II coefficient on the electric field and lattice temperature, we show in

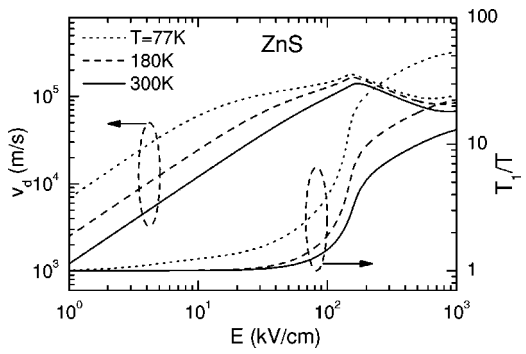

FIG. 3. Calculated electron drift velocity v_d of the whole system (left axis) and the normalized electron temperature, T_1/T, for the Γ valley (right axis) are shown as a function of the electric field E in ZnS at different lattice temperatures $T=77$, 180, and 300 K, respectively.

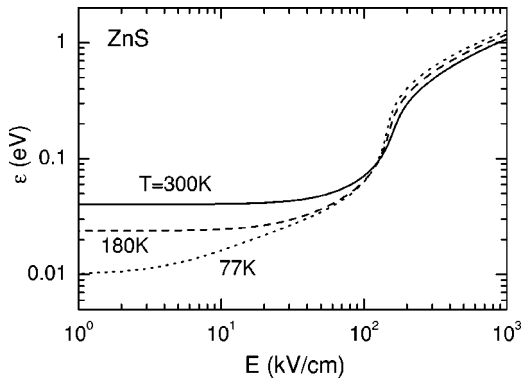

FIG. 4. Average electron energies are shown as a function of the electric field E in ZnS at different lattice temperatures $T=77$, 180, and 300 K, respectively.

Fig. 6 the calculated II coefficient α_{ii} of ZnS as a function of the inverse electric field at different lattice temperatures $T=77$, 180, and 300 K, respectively. It can be seen that the lower the lattice temperature, the larger the II coefficient is. At given field the electron temperature is higher at low lattice temperature. The reasons are as follows. As electrons accelerate under a given field, they quickly heat up. These hot electrons then collide frequently with phonons and relax to the quasiequilibrium state, thus reducing their temperature. How fast electrons lose their energy or how high electrons maintain their temperature is dependent on the phonon population, or the lattice temperature. If the lattice temperature is low, the phonon population is low and electron-phonon scattering is weak. As a result, electrons lose little energy and maintain a high electron temperature. We find that the dependence of the II coefficient on the electric field E can be fitted by the following exponential expression:

$$\alpha_{ii}=\alpha_0 \exp\left(-\frac{\beta_0}{E^{\gamma}}\right). \tag{14}$$

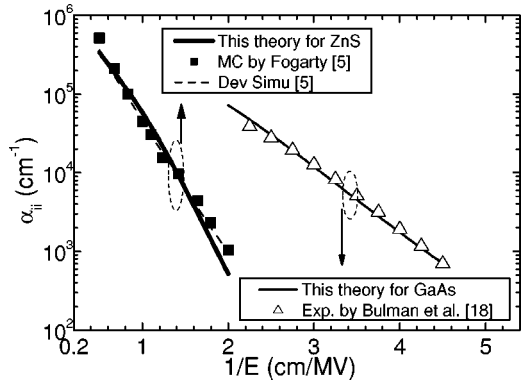

FIG. 5. Calculated II coefficient, α_{ii}, of ZnS (thick solid line) as a function of the inverse electric field at $T=300$ K. The solid squares is the EMC simulation results for ZnS from Ref. 5 and the thick dashed line shows the results from device modeling (Ref. 5). In addition, the calculated (thin solid line) and the experimental (open triangles) (Ref. 18) II coefficients for GaAs are also plotted for comparison.

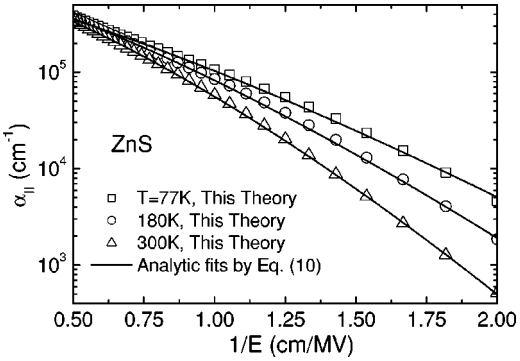

FIG. 6. Balance-equation calculated II coefficients (open symbols) α_{ii} of ZnS are shown as a function of the inverse electric field at different lattice temperatures $T=77$, 180, and 300 K, respectively. The solid lines show the corresponding analytic fits by Eq. (14).

The fitting parameters α_0, β_0, and γ for different lattice temperatures are presented in Table II. In Fig. 6 we have shown the fitting results (lines) by Eq. (14), which are in a good agreement with those (open symbols) obtained by numerically solving the balance Eqs. (1)–(3) in the field range 500 kV/cm$\leqslant E \leqslant$2000 kV/cm at lattice temperatures $T=77$, 180, and 300 K, respectively. The analytic expression by Eq. (14) for the dependence of the II coefficients on the electric field may be used in ZnS-based device modeling.

We notice that, all satellite valleys are anisotropic and thus become nonequivalent when they are coupled to an electrical field. For the present system we neglect this nonequivalence due to the following reasons. (1) There is only one satellite valley at Γ point, so we neglect the anisotropic effect when the electric field is along the [100] direction, (2) the X valley is most anisotropic. While most papers dealing with this problem use the isotropic approximation [see, e.g., Ref. 5, and references therein], it is expected that such isotopic approximation become less valid if a strong electric field is applied. However, since the electric field is along the [100] direction, the four satellite valleys (along [111], $[1\bar{1}1]$, $[11\bar{1}]$, and $[1\bar{1}\bar{1}]$) remain equivalent. Therefore, we assume the model of isotropic satellite valleys to be a good approximation, and (3) the three satellite valleys at L point will not remain equivalent under an electric field applied along [100]. However, two of the three satellite valleys are still equivalent. Since the energy of L point is higher than that of the X point and the anisotropic parameter for the L point is smaller compared to that of the X point. We shall neglect this anisotropic effect.

TABLE II. The fitting parameters for the II coefficients at different lattice temperatures T.

T (K)	α_0 (10^5 cm^{-1})	β_0	γ
77	8.09	2.06	1.3
180	9.33	2.43	1.35
300	9.94	2.88	1.4

IV. CONCLUSIONS

In conclusion, based on the nonparabolic multivalley balance equations extended to II process in semiconductors we have investigated electron transport properties and impact ionization effect in ZnS with a three-valley nonparabolic structure at high electric field up to 2000 kV/cm. Most important transport characteristics, such as electron velocity, electron energy, intervalley transfer, and impact ionization coefficient, are calculated by taking account of different scattering mechanisms with the inclusion of the impact ionization process. In the present approach the computational times required for getting accurate numerical results are quite acceptable when compared to MC simulation. The calculated results for average velocity and II coefficients are in agreement with recent MC results and the available experimental data, thus supporting the present nonparabolic multivalley balance-equation approach. In addition, we obtain an analytic formula for the field-dependent II coefficient, which may be directly used in modeling ZnS-based semiconductor device.

ACKNOWLEDGMENTS

This work was supported by the key National Natural Science Foundation of China (Grant No. 10390162), the Special Funds for Major State Basic Research Project (Project Nos. 2001CCA02800G and 20000683), and the Special Funds for Shanghai Optic Engineering (Grant Nos. 011661075 and 03JC14082). The author would like to thank Professor X. L. Lei for many helpful discussions.

[1] K. Brennan, J. Appl. Phys. **64**, 4024 (1988).
[2] M.V. Fischetti and S.E. Laux, Phys. Rev. B **38**, 9721 (1988).
[3] K. Bhattacharyya, S.M. Goodnick, and J.F. Wager, J. Appl. Phys. **73**, 3390 (1993).
[4] G.M. Dunn, G.J. Rees, J.P.R. David, S.A. Plimmer, and D.C. Herbert, Semicond. Sci. Technol. **12**, 111 (1997).
[5] J. Fogarty, W. Kong, and R. Solanki, Solid-State Electron. **38**, 653 (1995).
[6] M. Reigrotzki, Ph.D. thesis, University of Rostock, 1998.
[7] N. Fitzer, A. Kuligk, R. Redmer, M. Städele, S.M. Goodnick, and W. Schattke, Phys. Rev. B **67**, 201201 (2003).
[8] W. Shockley, Solid-State Electron. **2**, 35 (1961).
[9] P.A. Wolff, Phys. Rev. **95**, 1415 (1954).
[10] G.A. Baraff, Phys. Rev. **128**, 2507 (1962).
[11] B.K. Ridley, J. Phys. C **16**, 3373 (1983).
[12] S.P. Wilson, Solid-State Electron. **37**, 243 (1994).
[13] W. Quade, E. Schöll and M. Rudan, Solid-State Electron. **36**, 1493 (1993).
[14] X.F. Wang and X.L. Lei, J. Phys.: Condens. Matter **7**, 7871 (1995).

[15] J.C. Cao and X.L. Lei, Phys. Rev. B **67**, 085309 (2003).
[16] O. Madelung, W. von der Osten, and U. Rössler, in *Numerical Data and Functional Relationships in Science and Technology*, edited by O. Madelung, Landolt-Börnstein, New Series, Group III, Vol. 22, Pt. a (Springer, Berlin, 1987), p. 167.
[17] X.L. Lei, N.J.M. Horing, and H.L. Cui, Phys. Rev. Lett. **66**, 3277 (1991).
[18] G.E. Bulman, V.M. Robbins, and G.E. Stillman, IEEE Trans. Electron Devices **ED-32**, 2454 (1986).